Visualising Instabilities in Viscous, Continuously Stratified Parallel Flows

Hannah Swan

December 3, 2020

Abstract

The equations of motion for a non-rotating, Boussinesq fluid in the context of a continuously stratified parallel shear flow are described in terms of the Reynolds, Prandtl, and Richardson numbers. A viscous and diffusive analogue of the Taylor-Goldstein equation is derived which eliminates singularities that occur in the inviscid Taylor-Goldstein equation. Instabilities are simulated using hyperbolic tangent functions for the initial density profile and shear flow, with free slip and insulating boundary conditions. A variety of parameters are considered and billow development is discussed. It is shown that increasing the Reynolds number increases core strength of the billow, and increasing the Prandtl number has a similar effect. As expected from the physical meaning of the Richardson number, simulations performed at higher Richardson numbers are stabilized slightly, producing smaller billows than those seen in a weak stratification.

1 Introduction

Instabilities of density stratified fluids subject to a parallel shear flow are ubiquitous in nature, ranging from a primary instability which leads to turbulent mixing in the world's oceans [1], to instabilities on astrophysical scales in protoplanetary disks [2]. While Kelvin and Helmholtz only ever studied its discontinuously stratified counterpart, continuously stratified instability of this kind is also called Kelvin-Helmholtz instability. In the ocean, it is predominant in the density stratified regions of the interior, where internal gravity waves driven by wind and tidal forcing lead to internal wave shear. This shear ultimately counters the stable density stratification and leads to the growth of billows of rotating fluid which roll up the interface between two layers [3]. Turbulent patches develop when these billows break, ultimately mixing the fluid on a small scale.

Studies of continuously stratified Kelvin-Helmholtz instability began with Taylor and Richardson in 1915 and 1920 respectively. They both conjectured that for an inviscid, non-diffusive fluid experiencing gravitational acceleration g, with a reference density ρ_0, a background density stratification $\bar{\rho}(z)$, and a shear flow $\bar{u}(z)$, the quantity

$$Ri = \frac{g\frac{d\bar{\rho}}{dz}}{\rho_0(\frac{d\bar{u}}{dz})^2},$$

which is now known as the gradient Richardson number, must be everywhere greater than 1 for a fluid to be stable. Around the same time, Prandtl had argued that stability required $Ri > 2$. The arguments of all three provided upper bounds on the necessary condition for stability, but it was ultimately Miles and Howard who used linear stability arguments to deduce that a parallel shear flow is stable so long as $Ri > \frac{1}{4}$ everywhere in the fluid [4].

Neglecting viscous and diffusive effects comes with its fair share of challenges. While the damping effect of viscosity in parallel stratified shear flow is very small and the Richardson number remains the primary parameter in predicting instability even for viscous flows [5], the inviscid Taylor-Goldstein

equation is subject to singularities at critical points which make it challenging to solve numerically [6]. As will be discussed later, inclusion of viscosity and diffusion removes these singularities. Moreover, an inviscid, non-diffusive model is not realistic for real geophysical flows. To understand how these instabilities evolve in the world's oceans and atmosphere – and on astrophysical scales as well – these effects must be accounted for to get the whole picture. Thus, considering viscous and diffusive effects in the context of continuously stratified Kelvin-Helmholtz instability is worthwhile both for the purpose of modelling real geophysical flows and for removing singularities from stability calculations.

Following is a review of the equations of motion for a continuously stratified parallel flow, a derivation of a viscous and diffusive analogue of the Taylor-Goldstein equation, and discussion of the methodology behind two-dimensional simulations of the fluid flow. Visualisations of instability for a variety of Reynolds and Prandtl numbers will be presented, along with a discussion of how these parameters impact the evolution of Kelvin-Helmholtz instabilities.

2 Equations of Motion

Consider a non-rotating Boussinesq fluid wherein variations in density are considered negligible unless multiplied by the acceleration due to gravity. It is assumed the fluid is initially subjected to a shear flow $\bar{u}(z)$, and has a stable density stratification $\bar{\rho}(z)$ such that $\frac{d\bar{\rho}}{dz} < 0$. Letting the velocity field of the fluid be denoted by $\mathbf{u} = (u\ v\ w)^T$, pressure by p, density by ρ, and letting ν, κ, g, and ρ_0 represent the kinematic viscosity, diffusivity, acceleration due to gravity and a reference density respectively, the equations of motion for the fluid are

$$\frac{\partial \mathbf{u}}{\partial t} + \mathbf{u}\cdot\nabla\mathbf{u} = -\frac{1}{\rho_0}\nabla p + \nu\Delta\mathbf{u} - \frac{g}{\rho_0}\rho\hat{\mathbf{k}} \tag{1}$$

$$\nabla\cdot\mathbf{u} = 0 \tag{2}$$

$$\frac{\partial \rho}{\partial t} + \mathbf{u}\cdot\nabla\rho = \kappa\Delta\rho \tag{3}$$

Here $\hat{\mathbf{k}}$ is the unit vector in the positive z direction, and Δ is the Laplacian operator. Decomposing the density as $\rho = \rho_0 + \rho'$, where ρ' is the deviation from the reference density, and substituting into (1) – (3), gives

$$\frac{\partial \mathbf{u}}{\partial t} + \mathbf{u}\cdot\nabla\mathbf{u} = -\frac{1}{\rho_0}\nabla p + \nu\Delta\mathbf{u} - \frac{g}{\rho_0}\rho'\hat{\mathbf{k}} - g\hat{\mathbf{k}}$$

$$\nabla\cdot\mathbf{u} = 0$$

$$\frac{\partial \rho'}{\partial t} + \mathbf{u}\cdot\nabla\rho' = \kappa\Delta\rho'$$

The $g\hat{\mathbf{k}}$ term is absorbed into the pressure by defining $\hat{p} = p + g\rho_0 z$, so that $\nabla\hat{p} = \nabla p + g\rho_0\hat{\mathbf{k}}$. Thus the equations of motion are

$$\frac{\partial \mathbf{u}}{\partial t} + \mathbf{u}\cdot\nabla\mathbf{u} = -\frac{1}{\rho_0}\nabla\hat{p} + \nu\Delta\mathbf{u} - \frac{g}{\rho_0}\rho'\hat{\mathbf{k}} \tag{4}$$

$$\nabla\cdot\mathbf{u} = 0 \tag{5}$$

$$\frac{\partial \rho'}{\partial t} + \mathbf{u}\cdot\nabla\rho' = \kappa\Delta\rho' \tag{6}$$

A non-dimensional form of the equations will simplify the process of simulating the instability. The variables are scaled by taking

$$\mathbf{x} = h_0\mathbf{x}^* \qquad \mathbf{u} = u_0\mathbf{u}^* \qquad t = \frac{h_0}{u_0}t^* \qquad \rho' = r\rho^* \qquad \hat{p} = \rho_0 u_0^2 p^*$$

where h_0 is the initial thickness of the shear layer, and u_0 and $r = \rho_{bot} - \rho_{top}$ are respectively the velocity and density difference across it. Substituting the scaled variables into equations (4) – (6) and dropping the asterisks so that $\mathbf{x}$, $\mathbf{u}$, t, ρ and p all represent dimensionless quantities, the non-dimensional form of the equations of motion are expressed as

$$\frac{\partial \mathbf{u}}{\partial t} + \mathbf{u} \cdot \nabla \mathbf{u} = -\nabla p + \frac{1}{Re} \Delta \mathbf{u} - Ri \rho \hat{\mathbf{k}} \tag{7}$$

$$\nabla \cdot \mathbf{u} = 0 \tag{8}$$

$$\frac{\partial \rho}{\partial t} + \mathbf{u} \cdot \nabla \rho = \frac{1}{PrRe} \Delta \rho \tag{9}$$

where $Re = \frac{h_0 u_0}{\nu}$ is the initial Reynolds number of the flow, $Pr = \frac{\nu}{\kappa}$ is the Prandtl number, and $Ri = \frac{g r h_0}{\rho_0 u_0^2}$ is the Richardson number. The Reynolds number describes the relative importance of viscous effects, while the Prandtl number describes the ratio between momentum and density diffusivities. Finally, the Richardson number quantifies the importance of stratification and shear in the flow.

The problem is completed with a statement of the boundary conditions, and specification of the initial conditions $\bar{u}(z)$ and $\bar{\rho}(z)$. Shear and stratification concentrated in a layer of the dimensional form

$$\bar{u}(z) = \frac{u_0}{2} \tanh\left(\frac{2z}{h_0}\right) \qquad\qquad \bar{\rho}(z) = -\frac{r}{2} \tanh\left(\frac{2z}{\delta_0}\right),$$

where δ_0 is the initial thickness of the stratified density layer, are commonly chosen profiles when modelling instabilities of this type [7, 8, 9]. Together, this formulation of the initial conditions represents two streams of fluid travelling at different velocities with a smooth shear layer between them, where the upper fluid has lower density than the bottom layer, and the two form a smooth, stable density stratification. See Figure 1.

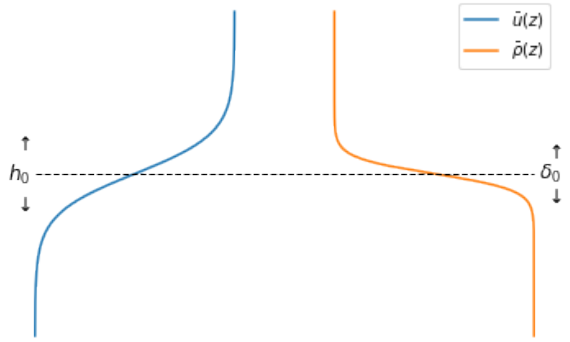

Figure 1: Density and shear velocity profiles used as the initial conditions for many simulations of continuously stratified Kelvin-Helmholtz instability, including those undertaken here.

These initial conditions are non-dimensionalized using the same scalings as outlined above, giving

$$\bar{u}^*(z) = \frac{1}{2} \tanh(2z^*) \qquad\qquad \bar{\rho}^*(z) = \frac{1}{2} \tanh(2Sz^*) \tag{10}$$

where the scale parameter $S = \frac{h_0}{\delta_0}$ describes the ratio between the thickness of the shear layer and density layer. A value of $S = 1$ is relevant to the case where thermal diffusion is considered, but molecular diffusion processes favour a thinner density layer relative to the shear layer, $S > 1$ [7]. The particular boundary conditions for the simulations performed here will be discussed in a later section.

3 The Viscous Taylor-Goldstein Equations

For a background shear $\bar{u}$, eigenfunction $\hat{\psi}$ and eigenvalue c, on a vertical domain $z \in (0, d)$, the Taylor Goldstein equation for an inviscid, non-diffusive fluid is given by

$$(c - \bar{u}(z)) \left(\frac{d^2}{dz^2} - k^2 \right) \hat{\psi} + \left(\frac{d^2 \bar{u}(z)}{dz^2} + \frac{N^2}{c - \bar{u}(z)} \right) \hat{\psi} = 0 \tag{11}$$
$$\hat{\psi}|_{z=0} = \hat{\psi}|_{z=d}$$

where $N^2 = -\frac{g}{\rho_0} \frac{d\bar{\rho}}{dz}$ is the square of the buoyancy frequency. It is a well studied problem describing the stability of stratified parallel flows. However, the neglect of viscosity, diffusion, and nonlinearities leads to singularities in the equation: inviscid shear flows satisfy Howard's semicircle theorem, which gives that the phase speed, $Re(c)$ lies between the minimum and maximum of the shear flow. Thus for a neutral mode, where c is real, there must be some point z_{cr} at which $\bar{u}(z_{cr}) = c$. This leads to a singularity in the Taylor-Goldstein equation and eigenfunctions which are discontinuous across the critical layer formed in the neighbourhood near the critical point z_c [10]. Including viscous and diffusive terms in the derivation is one method which can eliminate these singularities.

We begin with the equations of motion (1) – (3), but consider two dimensions only, as Squire's theorem guarantees that for stratified parallel shear flows, two dimensional perturbations are more unstable than three dimensional ones [10]. Formulated in terms of the buoyancy, $b = -\frac{g}{\rho_0}\rho$, the equations of motion become

$$\begin{aligned} \frac{\partial \mathbf{u}}{\partial t} + \mathbf{u} \cdot \nabla \mathbf{u} &= -\frac{1}{\rho_0} \nabla p + \nu \Delta \mathbf{u} + b\hat{\mathbf{k}} \\ \nabla \cdot \mathbf{u} &= 0 \\ \frac{\partial b}{\partial t} + \mathbf{u} \cdot \nabla b &= \kappa \Delta b \end{aligned}$$

We decompose the flow into the background components plus a perturbation, which are assumed small relative to the background:

$$u = \bar{u}(z) + u' \qquad w = w' \qquad b = b_0 + \bar{b}(z) + b' \qquad p = \bar{p}(x, z) + p'$$

At steady state, the background satisfies

$$\begin{aligned} -\frac{1}{\rho_0} \frac{\partial \bar{p}}{\partial x} + \nu \frac{d^2 \bar{u}}{dz^2} &= 0 \\ \frac{1}{\rho_0} \frac{\partial \bar{p}}{\partial z} &= -(b_0 + \bar{b}(z)) \\ \Delta \bar{b} &= 0 \end{aligned}$$

Using this decomposition and the above balances in (1) – (3), and neglecting terms nonlinear in the perturbations, we have

$$\frac{\partial u}{\partial t} + \bar{u}(z) \frac{\partial u}{\partial x} + w \frac{d\bar{u}}{dz} = -\frac{1}{\rho_0} \frac{\partial p}{\partial x} + \nu \Delta u \tag{12}$$
$$\frac{\partial w}{\partial t} + \bar{u}(z) \frac{\partial w}{\partial x} = -\frac{1}{\rho_0} \frac{\partial p}{\partial z} + b + \nu \Delta w \tag{13}$$
$$\frac{\partial u}{\partial x} + \frac{\partial w}{\partial z} = 0 \tag{14}$$
$$\frac{\partial b}{\partial t} + \bar{u}(z) \frac{\partial b}{\partial x} + w \frac{d\bar{b}}{dz} = \kappa \Delta b \tag{15}$$

Where it is understood that from here forward $u,\ w,\ b$, and p are the perturbation terms. Introducing the streamfunction ψ such that

$$u = -\frac{\partial \psi}{\partial z} \qquad\qquad w = \frac{\partial \psi}{\partial x}$$

and taking the curl of the momentum equations (12) and (13), we have

$$\left(\frac{\partial}{\partial t} + \bar{u}(z)\frac{\partial}{\partial x}\right)\Delta\psi - \frac{\partial \psi}{\partial x}\frac{d^2\bar{u}}{dz^2} = \frac{\partial b}{\partial x} + \nu\left(\frac{\partial^2}{\partial x^2} + \frac{\partial^2}{\partial z^2}\right)\Delta\psi \tag{16}$$

The buoyancy equation becomes

$$\frac{\partial b}{\partial t} + \bar{u}(z)\frac{\partial b}{\partial x} + \frac{\partial \psi}{\partial x}N^2 = \kappa\Delta b \tag{17}$$

Where we recognize that the buoyancy frequency is given by $N = \sqrt{\frac{d\bar{b}}{dz}}$. We seek plane wave solutions travelling the in direction of the shear:

$$\psi = \hat{\psi}(z)e^{i(kx-\omega t)} \qquad\qquad b = \hat{b}(z)e^{i(kx-\omega t)}$$

Substituting the above ansatz into (16) and (17) and dividing by $-ik$ leads to the Taylor-Goldstein equations with constant viscosity and diffusivity,

$$(c - \bar{u}(z))\left(\frac{d^2}{dz^2} - k^2\right)\hat{\psi} + \frac{d^2\bar{u}}{dz^2}\hat{\psi} = -\hat{b} + i\frac{\nu}{k}\left(\frac{d^2}{dz^2} - k^2\right)^2\hat{\psi} \tag{18}$$

$$(c - \bar{u}(z))\,\hat{b} - N^2\hat{\psi} = i\frac{\kappa}{k}\left(\frac{d^2}{dz^2} - k^2\right)\hat{b} \tag{19}$$

Where $c = \omega/k$. The boundary conditions are $\hat{\psi} = \hat{b} = 0$ at the upper and lower boundaries, and the additional condition of either $\frac{d\hat{\psi}}{dz} = 0$ or $\frac{d^2\hat{\psi}}{dz^2} = 0$ at the top and bottom [11]. Unlike the inviscid Taylor-Goldstein equation (11), equations (18) and (19) have no singularities and thus eigenfunctions are continuous on the domain. An alternative formulation of these equations in terms of the vertical velocity and buoyancy, which account for variable viscosity and diffusivity, are derived in [11]. Numerical solutions for these equations are explored in a variety of contexts by Lian *et al.* in [6]. In particular, the authors apply these equations to data taken from the Clyde sea, highlighting the fact that models including viscosity and diffusion are more realistic approximations to geophysical flows.

4 Simulations

Simulations of instabilities were performed using Dedalus, an open source python package for solving general partial differential equations using spectral methods [12]. The domain under consideration was a rectangle with aspect ratio 2, with length $L_x = 14$ and height $L_z = 7$. The size of the domain was chosen to allow billows to form without interference from the boundaries. The horizontal basis was chosen to be Fourier and the vertical basis was chosen to be Chebyshev, which allowed for enforcement of the free-slip boundary conditions and use of the Fast Fourier Transform for computational efficiency. Timestepping was performed using a four-stage, third order implicit-explicit Runge-Kutta method. Equations (7) – (9) were solved in two-dimensions with initial conditions (10). The sidewalls of the domain were considered periodic, while free-slip, insulating boundaries were chosen at the top and bottom walls:

$$w|_{z=\pm L_z/2} = \frac{\partial u}{\partial z}|_{z=\pm L_z/2} = 0 \qquad\qquad \frac{\partial \rho}{\partial z}|_{z=\pm L_z/2} = 0$$

Along with the specified shear flow and background stratification, a perturbation to the vertical velocity was introduced as an initial condition. In particular, a single mode was excited for all but one simulation. The final simulation excited two modes.

Simulations were performed at a variety of parameter values as indicated in Table 1. The Prandtl numbers selected are representative of thermal diffusion in the atmosphere ($Pr = 0.72$) and thermal diffusion in water ($Pr = 7$). Variation in the Reynolds number effectively varies the strength of the viscosity, thus allowing for comparison. Two values of the Richardson number were selected to allow for observation of the effects of weak and moderate density stratification [13]. Finally, as both Prandtl numbers chosen represent thermal diffusion, the scale parameter S was fixed at 1 for all simulations.

Simulation	1	2	3	4	5	6*
Re	1300	800	1300	1300	5000	3000
Pr	0.72	7	7	7	7	7
Ri	0.035	0.035	0.035	0.08	0.08	0.08
S	1	1	1	1	1	1

Table 1: Parameter values for 2D simulations performed. The starred simulation is the only simulation which had more than one excited mode in the initial condition.

4.1 The Life Cycle of a Kelvin-Helmholtz Instability

As the instability in a stratified shear layer develops, it forms regions of rotating fluid called billows. Each billow has a core of concentrated vorticity, each connected to the next by a thin, tilted strip containing vorticity. This strip is known as the braid. The billow advects vorticity into its core, growing until it reaches a saturation point. After saturation, a billow may form a vortex pair with a neighbouring billow, or in the absence of this so-called vortex pairing, it will simply continue to exchange energy with the background without changing in size. Up to this point, the growth of the billow is purely two-dimensional, but with the development of three-dimensional instabilities the billow eventually transitions into turbulence [8]. The structure of a developed instability is shown in Figure 2 below, indicating the core and braid regions, as well as an instance of vortex pairing.

The energy exchange that occurs during the development of instability can be ascertained through numerical simulations. Let $\langle\cdot\rangle_p$ denote an average over the p-dimension of the domain, so that, for example

$$\langle f(x,z,t)\rangle_{xz} = \frac{1}{L_x L_z}\int_{-L_z/2}^{L_z/2}\int_0^{L_x} f(x,z,t)dxdz$$

Then we can write the volume-averaged total kinetic energy per unit mass of the system as

$$K = \frac{1}{2}\langle u^2 + w^2\rangle_{xz}$$

Following [13], the total kinetic energy can be broken down into $K = \bar{K} + K_{2D}$ which are respectively the average kinetic energy of the mean background flow, and the average kinetic energy of the perturbation. Using the horizontally averaged velocity,

$$\bar{\mathbf{U}}(z,t) = \langle \mathbf{u}\rangle_x = \bar{U}(z,t)\hat{\mathbf{i}}$$

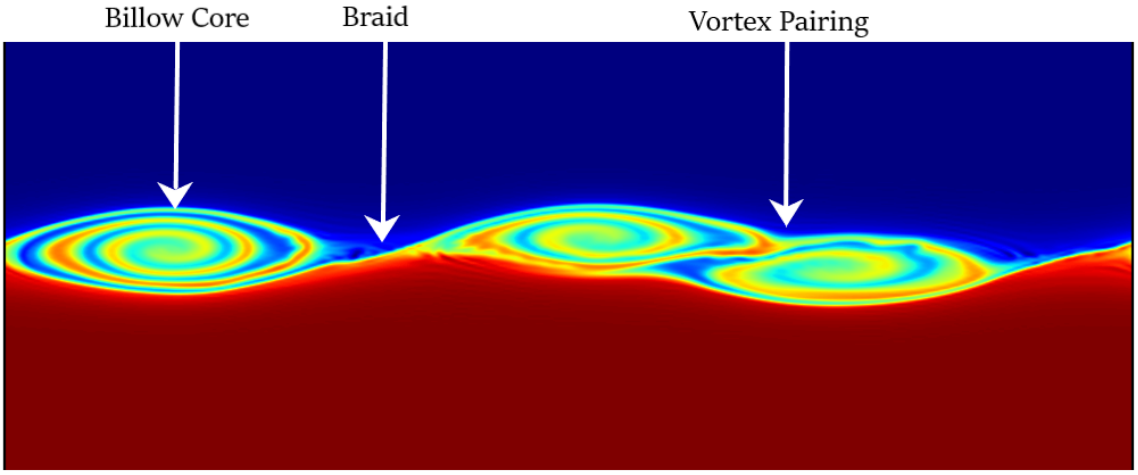

Figure 2: Structure of a continuously stratified Kelvin-Helmholtz instability, showing the billow cores, braid and vortex pairing. This image shows a snapshot of the density field of Simulation 6 in Table 1.

where it follows from the incompressibility condition on the fluid that the horizontal average of the vertical velocity is zero, $\bar{K}$ and K_{2D} are given as

$$\bar{K} = \frac{1}{2}\langle \bar{U}^2 \rangle_z$$
$$K_{2D} = \frac{1}{2}\langle (\mathbf{u} - \bar{\mathbf{U}}) \cdot (\mathbf{u} - \bar{\mathbf{U}}) \rangle_{xz}$$

The total volume-averaged potential energy per unit mass of the system is expressed as

$$P = Ri\langle \rho z \rangle_{xz}$$

The kinetic and potential energy plots for a billow development prior to the onset of vortex pairing are shown in Figure 3 below. The total kinetic energy decreases with time, which is to be expected as energy is lost to viscous dissipation. Conversely, we see the potential energy increase with time, peaking at time t_2 as lighter fluids are pushed down and heavier fluids are forced upwards during the roll-up of the billow. The oscillations present in the time series of the total kinetic and potential energies can be attributed to the reversible exchange of kinetic and potential energy as the billow grows. As for K_{2D}, it experiences almost exponential growth up to its maximum, marked time t_1 on the figure. This time coincides with when the billow is nearest to a circular shape [13]. The oscillations seen in K_{2D} are due to the exchange of kinetic energy between the perturbation and the background.

In the event that a billow undergoes vortex pairing with a neighbouring billow, K_{2D} once again rises to a peak, followed by a maximum in the potential energy. Subsequent oscillations of kinetic and potential energy once again appear, albeit at higher energies than those observed prior to vortex pairing. Figure 4 shows the energy plots of the same simulation as Figure 3, but including the formation of a vortex pair. Times t_3 and t_4 are respectively the maximum of the perturbation kinetic energy and the potential energy after the onset of vortex pairing.

Snapshots of the density field for the fluid at the times t_1, t_2, t_3, and t_4 are shown in Figure 5. One can see that at times t_1 and t_3 where K_{2D} is at a maximum the billow is round and near-circular, elongating to an ellipse as it transitions to times t_2 and t_4 where potential energy is at a maximum. The paired vortices are clearly visible in the billow pictured at time t_3.

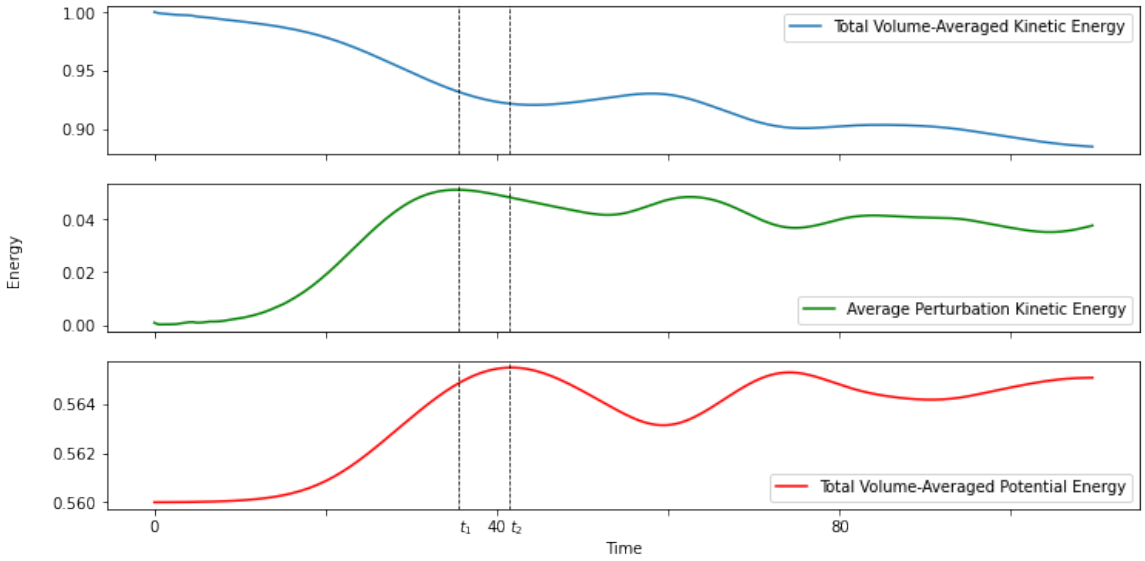

Figure 3: Plots of the total volume-averaged kinetic energy, average perturbation kinetic energy (both normalized by $K(0)$), and potential energy for the development of a Kelvin-Helmholtz instability prior to the onset of vortex pairing. The data presented here was collected in Simulation 4 in Table 1.

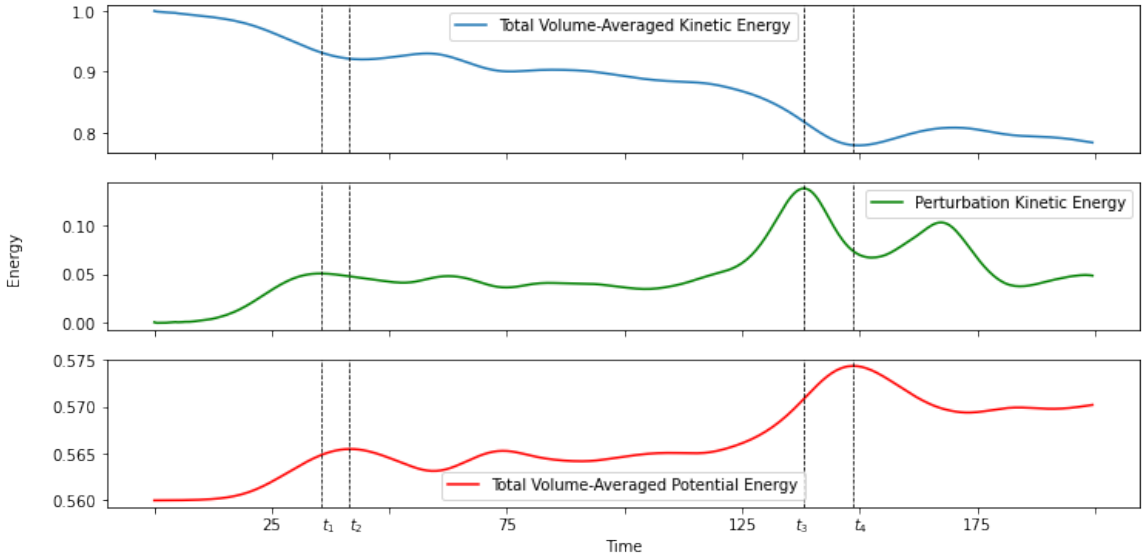

Figure 4: Plots of the total volume-averaged kinetic energy, perturbation kinetic energy (both normalized by $K(0)$), and the potential energy for the development of the primary Kelvin-Helmholtz instability, followed by the onset and development of vortex pairing.

While two-dimensional instabilities of this type are never truly turbulent, they do still serve to mix the fluid. In experiments performed by Caulfield and Peltier in [13], it was found that the primary mixing events occurred in the statically unstable regions of the billows generated as the billow core rotated, and thus the primary mechanism for mixing in such two-dimensional flows is

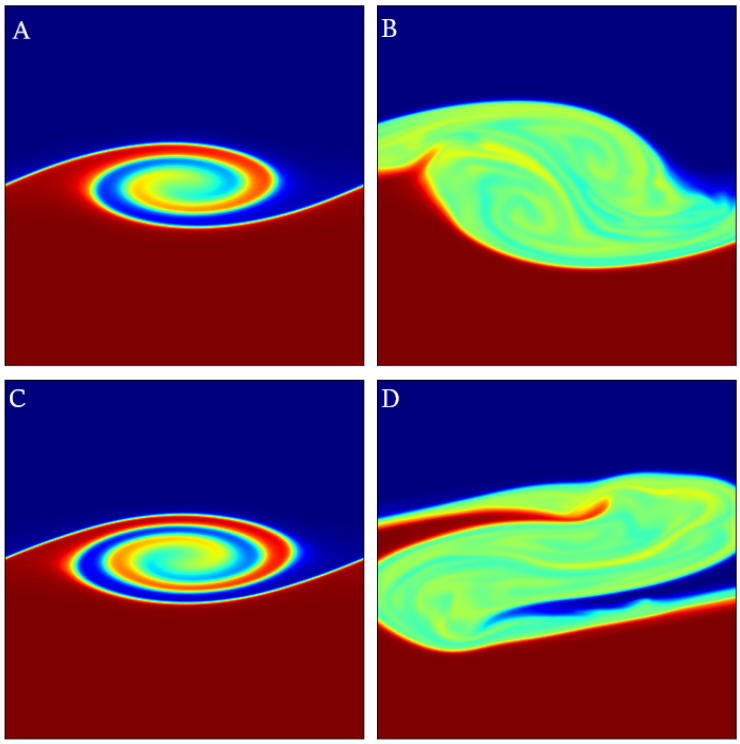

Figure 5: Density snapshots of Kelvin-Helmholtz billows taken from simulation 4 in Table 1 at the times A: t_1, B: t_3, C: t_2, and D: t_4 as indicated in the plots in Figures 3 and 4. The aspect ratios of all snapshots are the same.

associated with the roll-up of the billow.

4.2 Influence of Re, Pr, and Ri

Figure 6 shows the density and vorticity of three simulations of varying Reynolds number. As seen in the third row of snapshots, at a higher Reynolds number - associated with low viscosity - the billow grows faster, reaching saturation and becoming subject to secondary instabilities before the simulations performed at lower Reynolds numbers. At high Reynolds number less viscous diffusion of vorticity occurs, allowing the cores and braids to become more highly concentrated and thus leading to faster growth. Conversely, at lower Reynolds numbers we see a less concentrated, spread-out core which is indicative of the recirculation of vorticity between the core and the braid as a result of viscous diffusion. The results observed here are supported by previous, similar studies in [8].

To visualize the effects of the Prandtl number on the development of Kelvin-Helmholtz instabilities, two simulations at different Prandtl numbers but with fixed Reynolds and Richardson numbers are compared in Figure 7. Initially the billows evolve similarly, with their differences becoming very evident in the third snapshot. The diffusion timescale is long compared to the timescale for the evolution of the billow, hence why diffusive effects take longer to appear. Both the density and vorticity snapshots show that the billow cores of the lower Prandtl number fluid are much less structured than those of the higher Prandtl number fluid. As noted by [8], the increase in structure at high Pr is due to the increased baroclinic generation of vorticity as there is less diffusion of density. While Prandtl numbers higher than 7 were not achieved here, studies with Prandtl numbers as high as 700 further noted that the billows at such a high Prandtl number rose higher and the braids were

more steeply tilted, indicating a stronger core as in the case of high Reynolds number. Finally, small regions of negative vorticity are visible on the edges of the billow in the snapshots at $Pr = 7$. This effect is more pronounced at higher Prandtl numbers and serves to limit recirculation of vorticity from the core to the braid [8].

The Richardson number quantifies the strength of the stratification of the fluid. Given that the fluid is stably stratified, we expect that the moderate Richardson number of 0.08 will have a stabilizing effect over the weak stratification represented by the Richardson number of 0.035. From the snapshots presented in Figure 8, we see that this is, in fact the case. The higher Richardson number fluid produces smaller, shorter billows which indicates the stabilizing effect we expected.

5 Conclusions

To resolve singularities in the Taylor Goldstein equation for the linear stability of a parallel shear flow, viscous and diffusive effects were considered. The result was a system of coupled ordinary differential equations of higher order than the inviscid Taylor-Goldstein equation, but which produces continuous solutions and is applicable to real geophysical flows.

Continuously stratified Kelvin-Helmholtz instabilities were simulated using the non-rotating Boussinesq equations non-dimensionalized in terms of the Reynolds, Prandtl and Richardson numbers. The initial thickness of the shear and density layers were taken to be equal to simulate the effects of thermal diffusion at the Prandtl numbers of the atmosphere and water. As Kelvin-Helmholtz billows evolved, computations of the mechanical energy of the system showed decreasing kinetic energy over time, with oscillations in the kinetic and potential energy observed due to the reversible exchange between the two. The kinetic energy of the perturbation was found to rise to a peak when the billow was the most round, subsequently oscillating as the billow exchanged kinetic energy with the mean background flow.

When varying the Reynolds number, it was found that the lower viscous diffusion of vorticity that occurs at higher Reynolds numbers produced a stronger billow core, causing the billow to reach its saturation point and become subject to secondary instabilities sooner than the case of low Reynolds number. Conversely, at low Reynolds numbers, viscous diffusion lead to recirculation of vorticity from the core to the braid which contributed to a weaker core. Similar to the Reynolds number, increasing the Prandtl number lead to a stronger billow core which presented more structure compared to the diffuse core of the low Prandtl number fluid. The appearance of negative vorticity wrapping around the core at higher Prandtl number served to prevent recirculation of vorticity. It was particularly noted that the effects of density diffusion did not immediately appear in the evolution of the billows due to the discrepancy in the timescales for billow evolution and diffusion. Finally, as was expected from the physical meaning of the Richardson number, a more strongly stratified fluid presented smaller billows which indicated the stabilizing effects of density stratification.

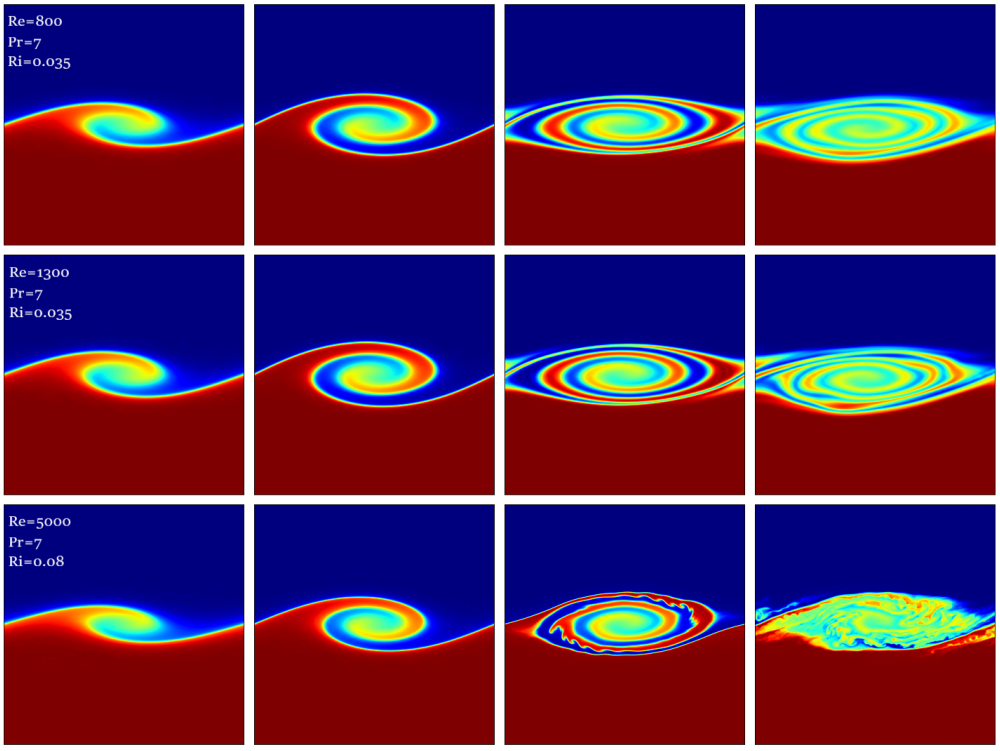

(a) Density field of simulations 2, 3, and 5 in Table 1.

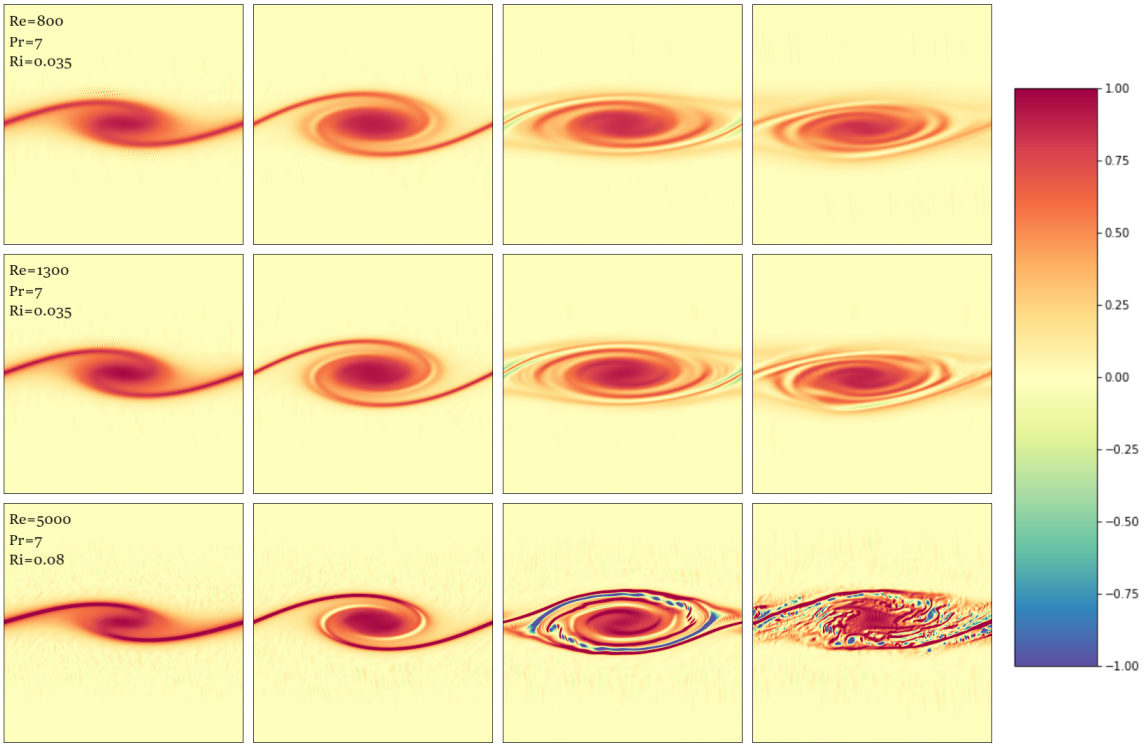

(b) Vorticity of simulations 2, 3, and 5 in Table 1.

Figure 6: Snapshots of simulations of varying Reynolds number at dimensionless times $t = 20, 30, 50, 80$.

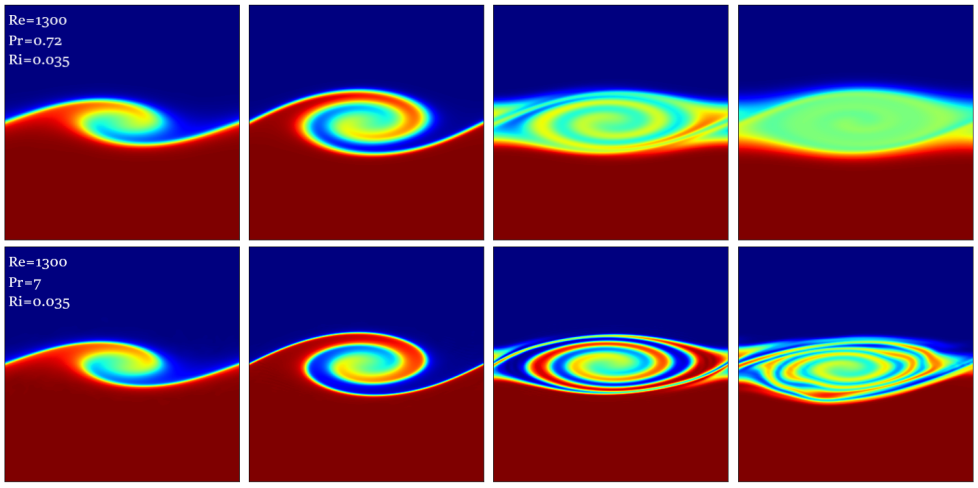

(a) Density field of simulations 1 and 3 in Table 1.

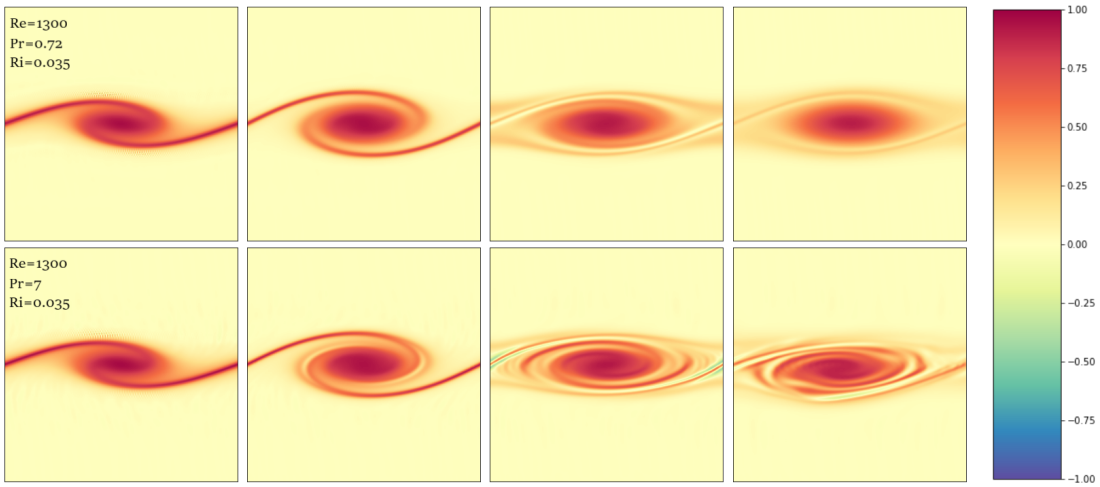

(b) Vorticity of simulations 1 and 3 in Table 1.

Figure 7: Snapshots of simulations of varying Prandtl number at dimensionless times $t = 20, 30, 50, 80$.

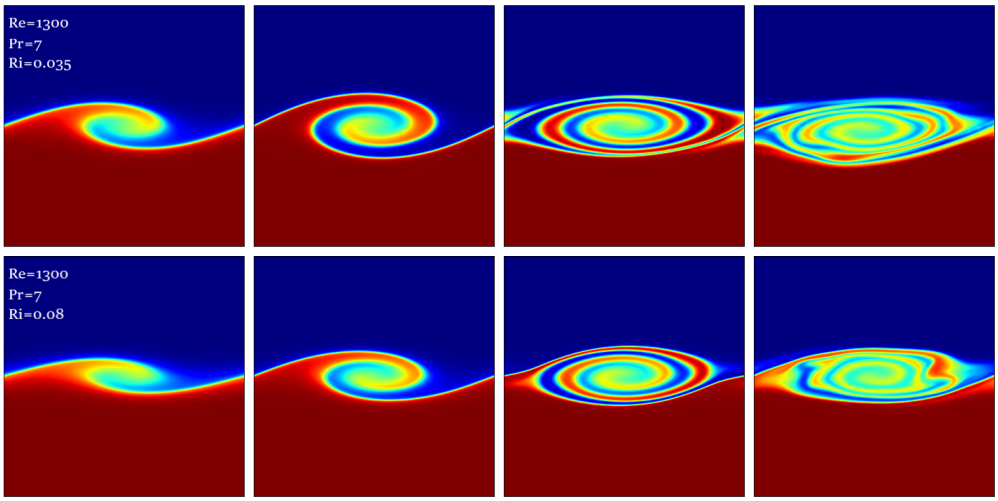

(a) Density field of simulations 3 and 4 in Table 1.

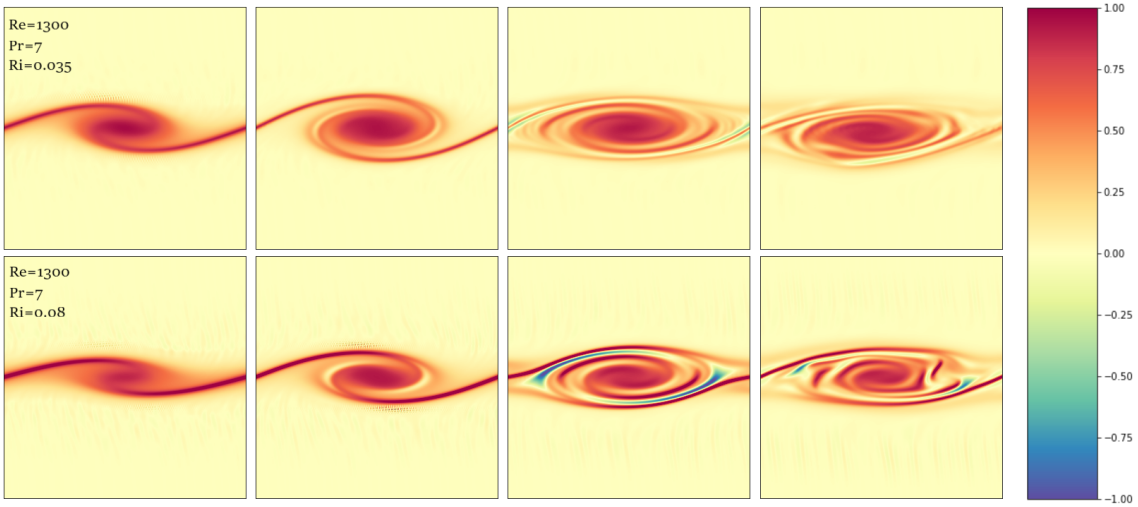

(b) Vorticity of simulations 3 and 4 in Table 1.

Figure 8: Snapshots of simulations of varying Richardson number at dimensionless times $t = 20, 30, 50, 80$.

References

[1] H. van Haren and L. Gostiaux, "A deep-ocean Kelvin-Helmholtz billow train," *Geophysical Research Letters*, vol. 37, pp. n/a–n/a, feb 2010.

[2] A. Johansen, T. Henning, and H. Klahr, "Dust Sedimentation and Self-sustained Kelvin-Helmholtz Turbulence in Protoplanetary Disk Midplanes," *The Astrophysical Journal*, vol. 643, pp. 1219–1232, jun 2006.

[3] W. Smyth and J. Moum, "Ocean Mixing by Kelvin-Helmholtz Instability," *Oceanography*, vol. 25, pp. 140–149, jun 2012.

[4] J. Miles, "Richardson's criterion for the stability of stratified shear flow," *Physics of Fluids*, vol. 29, no. 10, p. 3470, 1986.

[5] S. A. Maslowe, "Stability of a Stratified Free Shear Layer," *Physics of Fluids*, vol. 14, no. 3, p. 453, 1971.

[6] Q. Lian, W. D. Smyth, and Z. Liu, "Numerical Computation of Instabilities and Internal Waves from In Situ Measurements via the Viscous Taylor–Goldstein Problem," *Journal of Atmospheric and Oceanic Technology*, vol. 37, pp. 759–776, apr 2020.

[7] W. D. Smyth and J. N. Moum, "Length scales of turbulence in stably stratified mixing layers," *Physics of Fluids*, vol. 12, pp. 1327–1342, jun 2000.

[8] M. Rahmani, B. Seymour, and G. Lawrence, "The evolution of large and small-scale structures in Kelvin–Helmholtz instabilities," *Environmental Fluid Mechanics*, vol. 14, pp. 1275–1301, feb 2014.

[9] P. Hazel, "Numerical studies of the stability of inviscid stratified shear flows," *Journal of Fluid Mechanics*, vol. 51, pp. 39–61, jan 1972.

[10] P. Kundu, *Fluid Mechanics*. Amsterdam Boston: Academic Press, fourth ed., 2008.

[11] Z. Liu, S. A. Thorpe, and W. D. Smyth, "Instability and hydraulics of turbulent stratified shear flows," *Journal of Fluid Mechanics*, vol. 695, pp. 235–256, feb 2012.

[12] K. J. Burns, G. M. Vasil, J. S. Oishi, D. Lecoanet, and B. P. Brown, "Dedalus: A flexible framework for numerical simulations with spectral methods," *Physical Review Research*, vol. 2, apr 2020.

[13] C. P. Caulfield and W. R. Peltier, "The anatomy of the mixing transition in homogeneous and stratified free shear layers," *Journal of Fluid Mechanics*, vol. 413, pp. 1–47, jun 2000.